# Supplementary material for "A noninvasive and nonadiabatic quantum Maxwell demon"

Lucas Trigal[1, 2] and Rafael Sánchez[2, 3, 4]

[1] *Instituto de Física Interdisciplinar y Sistemas Complejos IFISC (CSIC-UIB), E-07122 Palma de Mallorca, Spain*
[2] *Departamento de Física Teórica de la Materia Condensada, Universidad Autónoma de Madrid, 28049 Madrid, Spain*
[3] *Condensed Matter Physics Center (IFIMAC), Universidad Autónoma de Madrid, 28049 Madrid, Spain*
[4] *Instituto Nicolás Cabrera (INC), Universidad Autónoma de Madrid, 28049 Madrid, Spain*

(Dated: November 3, 2025)

In this supplementary material we give details of the evolution equations in the different stages of the protocol as well as a heuristic model that describes the main features of the numerical simulations in the main text and provides analytical understanding of the involved processes.

## PROTOCOL STEPS

In this appendix, we detail the procedure used to simulate stochastic quantum-jump trajectories via the Monte Carlo wavefunction method [1]. We denote by $\rho_{n-1}$ the state of the double quantum dot (DQD) just after the $(n-1)$th detection event at time $t_{n-1}$. Initially, the DQD is empty:

$$\rho_0 = |0\rangle\langle 0|.$$

1. **No-jump evolution and sampling the jump time.**
   Draw a uniform random number $r \in [0,1]$. Propagate $\rho_{n-1}$ under the "no-jump" superoperator

   $$\mathcal{L}_0(\rho) = -i\big[H_0,\,\rho\big]\,dt \;-\; \sum_{i=+,-} \mathbb{M}_i(\rho)\,dt,$$

   where $\mathbb{M}_i(\rho)$ is defined in Eq. (3) of the main text. At each time step compute the survival probability

   $$P_{\rm surv}(t) = \mathrm{Tr}\big\{e^{\mathcal{L}_0\,t}\,\rho_{n-1}\big\}.$$

   When $P_{\rm surv}(\tau_n) = r$, declare $\tau_n$ the waiting time for the $n$th jump, set

   $$t_n = t_{n-1} + \tau_n, \quad \rho_n^* = \frac{e^{\mathcal{L}_0\,\tau_n}\,\rho_{n-1}}{\mathrm{Tr}\{e^{\mathcal{L}_0\,\tau_n}\,\rho_{n-1}\}},$$

   and proceed to the jump. We do not distinguish which dot becomes occupied—only whether the DQD is empty or not. Thus, immediately after the jump the state is

   $$\rho_n = \sum_{k=l,r} \frac{L_k^{\rm in}\,\rho_n^*\,\big(L_k^{\rm in}\big)^\dagger}{\mathrm{Tr}\{L_k^{\rm in}\,\rho_n^*\,\big(L_k^{\rm in}\big)^\dagger\}} = \frac{f_l\,|l\rangle\langle l| \;+\; f_r\,|r\rangle\langle r|}{f_l + f_r},$$

   where $L_k^{\rm in} = \sqrt{\Gamma\,f_k(\varepsilon_k)}\;|k\rangle\langle 0|$.

2. **Decoupling and driven evolution.**
   Immediately after detection, switch off tunneling ($\Gamma \to 0$) and sweep the dot energies linearly through the avoided crossing. The state $\rho_n$ then evolves under

   $$\dot\rho = \mathcal{L}_d(\rho) = -\,i\big[H_0(t),\,\rho\big].$$

   Integrating for a duration $\tau_d$ gives

   $$\rho_n(t_n+\tau_d) = \frac{e^{\mathcal{L}_d\,\tau_d}\,\rho_n(t_n)}{\mathrm{Tr}\{e^{\mathcal{L}_d\,\tau_d}\,\rho_n(t_n)\}}.$$

3. **Re-coupling and the next jump.**
   Re-enable tunneling to the reservoirs and repeat steps 1–3, now starting from the occupied state $\rho_n(t_n+\tau_d)$. Draw a new random number $r'$, propagate under $\mathcal{L}_0$ until $\mathrm{Tr}\{e^{\mathcal{L}_0\,\tau_{n+1}}\,\rho_n(t_n+\tau_d)\} = r'$, record $\tau_{n+1}$, and reset the DQD to the empty state $|0\rangle\langle 0|$.

## HEURISTIC MODEL

We can write a simple model based on a rate equation for sequential transitions between an enlarged Hilbert space. It considers the empty state $|0\rangle$, and $|l\rangle$, $|r\rangle$ for states before the driving, and $|l^*\rangle$, $|r^*\rangle$ for states after the driving. The successful transitions $|l\rangle \to |r^*\rangle$ and $|r\rangle \to |l^*\rangle$ have a rate $\gamma_{LZ} = P_{LZ}/\tau_d$, and the errors $|l\rangle \to |l^*\rangle$ and $|r\rangle \to |r^*\rangle$ a rate $\bar\gamma_{LZ} = (1-P_{LZ})/\tau_d$. Assuming that the detection of tunneling through the contacts to the reservoirs is instantaneous, the transitions $|L\rangle \to |0\rangle$ and $|R\rangle \to |0\rangle$ are avoided, hence explicitly breaking detailed balance. We furthermore assume that the splitting is large enough for the interdot overlap to be negligible during the detection stages, $\Delta_\varepsilon \gg \Omega$ [2]. Then a local description in terms of localized states is convenient [3].

The transfer probability, $P_{LZ}$, is obtained by propagating the initial state $\hat\rho(t_0) = (f_L^0, f_R^\Delta)\mathbb{1}_2/(f_L^0 + f_R^\Delta)$ during the drive stage via the von Neumann equation $\dot{\hat\rho}(t) = [\hat H_0(t), \hat\rho(t)]/i\hbar$, such that $P_{LZ} \equiv \rho_{rr}(t_0+\tau_d)$. The Fermi functions $f_j^0 = 1/\{1+\exp[(\varepsilon_0-\mu_j)/k_{\rm B}T]\}$ and $f_j^\Delta = 1/\{1+\exp[(\varepsilon_0+\Delta_\varepsilon-\mu_j)/k_{\rm B}T]\}$ give the occupation of the reservoirs at the tunneling energies. The result is plotted in Fig. S1 for two different temperatures

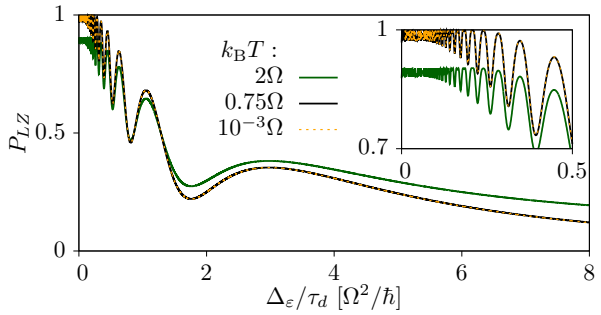


FIG. S1. Occupation probability of the right dot after going through the avoided crossing at a speed $\Delta_\varepsilon/\tau_d$, for $\varepsilon_0 = -0.5\Omega$ and $\Delta_\varepsilon = 6\Omega$, for three different temperatures of the reservoirs, $k_BT = (10^{-3}, 0.75, 2)\Omega$, and $\Delta\mu = 0$. The lower temperature curves are almost identical. The inset zooms in the adiabatic regime.

of the system at $\Delta\mu = 0$. As temperature increases, the initial occupation of $|r\rangle$ reduces $P_{LZ}$ and hence the confidence of the demon in the driving.

With this and the Fermi golden rule transition rates $\Gamma^+_{L0} = \Gamma_L f^0_L$ and $\Gamma^+_{R\Delta} = \Gamma_R f^\Delta_R$ for tunneling in (via transitions $|0\rangle \to \{|l\rangle, |r\rangle\}$, respectively), and $\Gamma^-_{L\Delta} = \Gamma_L(1 - f^\Delta_L)$ and $\Gamma^-_{R0} = \Gamma_R(1 - f^0_R)$ for tunneling out (via $\{|l^*\rangle, |r^*\rangle\} \to |0\rangle$), the master equation for the occupations $p_j = \rho_{jj}$ reads:

$$\begin{aligned}
\dot{p}_0 &= \Gamma^-_{R0} p_{r^*} + \Gamma^-_{L\Delta} p_{l^*} - (\Gamma^+_{l0} + \Gamma^+_{R\Delta}) p_0 \\
\dot{p}_l &= \Gamma^+_{L0} p_0 - \tau_d^{-1} p_l \\
\dot{p}_r &= \Gamma^+_{R\Delta} p_0 - \tau_d^{-1} p_r \\
\dot{p}_{l^*} &= \bar{\gamma}_{LZ} p_l + \gamma_{LZ} p_r - \Gamma^-_{L\Delta} p_{l^*} \\
\dot{p}_{r^*} &= \gamma_{LZ} p_l + \bar{\gamma}_{LZ} p_r - \Gamma^-_{R0} p_{r^*},
\end{aligned} \tag{S1}$$

where $\Gamma_L$ and $\Gamma_R$ are the transparencies of the barriers connecting the DQD to reservoirs L and R.

In the stationary regime, $\dot{p}_j = 0$, the particle current, $I = \Gamma^-_{R0} p_{r^*} - \Gamma^+_{R\Delta} p_0$, becomes:

$$I = \frac{P_{LZ}(\Gamma^+_{L0} - \Gamma^+_{R\Delta})\Gamma^-_{L\Delta}\Gamma^-_{R0}}{\tau_d \Lambda_3}, \tag{S2}$$

where $\Lambda_3 \equiv (\tau_d^{-1} + \Gamma^+_{R\Delta} + \Gamma^+_{L0})\Gamma^-_{L\Delta}\Gamma^-_{R0} + \tau_d^{-1}[\Gamma^-_{R0}\Gamma^+_{L0} + \Gamma^-_{L\Delta}\Gamma^+_{R\Delta} + P_{LZ}(\Gamma^+_{L0} - \Gamma^+_{R\Delta})(\Gamma^-_{L\Delta} - \Gamma^-_{R0})]$. The second term within parenthesis in Eq. (S2) accounts for unwanted transitions that are undetectable to the demon. However, in the appropriate configuration with $\varepsilon_0 + \Delta_\varepsilon \gg \mu_R, k_BT$, we have $\Gamma^+_{L0} \gg \Gamma^+_{R\Delta}$. Additionally, in the adiabatic regime, $\gamma_{LZ} \to \tau_d^{-1}$ and $\bar{\gamma}_{LZ} \to 0$, resulting in an error-free current:

$$I_{\mathrm{e-f}} = \left(\tau_s + \frac{1}{\Gamma^+_{L0}} + \frac{1}{\Gamma^-_{R0}}\right)^{-1}. \tag{S3}$$

The current in Eq. (S2) is plotted in Fig. S2 and compared with the numerical results shown in Fig. 2 of the main text for the same parameters, with very good agreement. The low speed linear dependence reproduces the result of Eq. (S3), see black dotted line in the rightmost panel of Fig. S2.

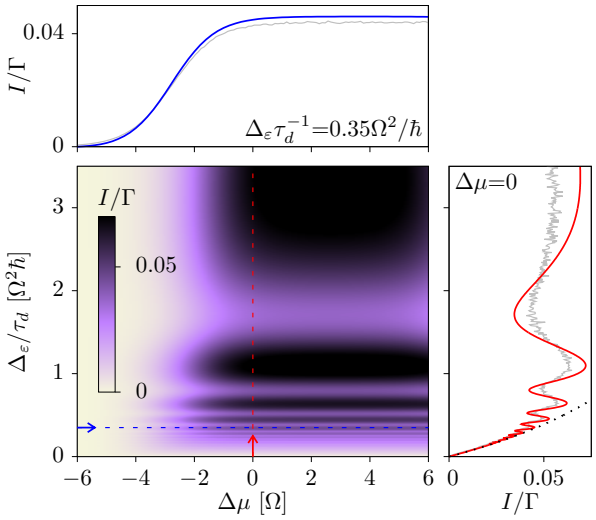


FIG. S2. Average particle current through the DQD computed with the heuristic model as a function of the applied electrochemical potential bias and the speed of the energy ramp, with cuts along the marked dotted lines plotted in the lateral panels. $\Gamma = \Omega/\hbar$, $T_l = T_r = 0.75\Omega/k_B$, $\varepsilon_0 = -0.5\Omega$, $\mu_r = 0$, $\Delta = 6\Omega$. In the lateral panels, the model is compared to the numerical results in Fig. 2 of the main text (grey lines). The black dotted line in the rightmost panel plots Eq. (S3).

### Thermal currents

We can also calculate the heat currents, $J_L = (\varepsilon_0 - \mu_L)\Gamma^+_{L0} p_0 - (\varepsilon_0 + \Delta_\varepsilon - \mu_L)\Gamma^-_{L\Delta} p_{l^*}$ and $J_R = (\varepsilon_0 + \Delta_\varepsilon - \mu_R)\Gamma^+_{R\Delta} p_0 - (\varepsilon_0 - \mu_R)\Gamma^-_{R0} p_{r^*}$, the generated power, $P = (\mu_R - \mu_L)I$, and the work performed by the demon due to the unsuccessful driving events, $\dot{W}_d = \Delta_\varepsilon \bar{\gamma}_{LZ}(p_l - p_r)$. The resulting expressions

$$J_L = \frac{(\varepsilon_0 - \mu_L)\Gamma^+_{L0} - (\varepsilon_1 - \mu_L)\Gamma^+_{R\Delta} - \eta_{LZ}\Delta_\varepsilon\Gamma^+_{L0}}{\Gamma^+_{L0} - \Gamma^+_{R\Delta}} I \tag{S4}$$

$$J_R = \frac{(\varepsilon_1 - \mu_R)\Gamma^+_{R\Delta} - (\varepsilon_0 - \mu_L)\Gamma^+_{L0} + \eta_{LZ}\Delta_\varepsilon\Gamma^+_{R\Delta}}{\Gamma^+_{L0} - \Gamma^+_{R\Delta}} I \tag{S5}$$

$$\dot{W}_d = \eta_{LZ}\Delta_\varepsilon I \tag{S6}$$

explicitly verify the first law $J_L + J_R + \dot{W}_d = P$, where $\varepsilon_1 \equiv \varepsilon_0 + \Delta_\varepsilon$ and $\eta_{LZ} = (1 - P_{LZ})/P_{LZ}$ is the driving error rate.

In Fig. S3 we plot the thermal currents. The model reproduces all the features described in the main text, including the cooling in L and R, power generation for $\Delta\mu < 0$ and the suppression of the driving work in the adiabatic regime. For large and positive $\Delta\mu$, the particle

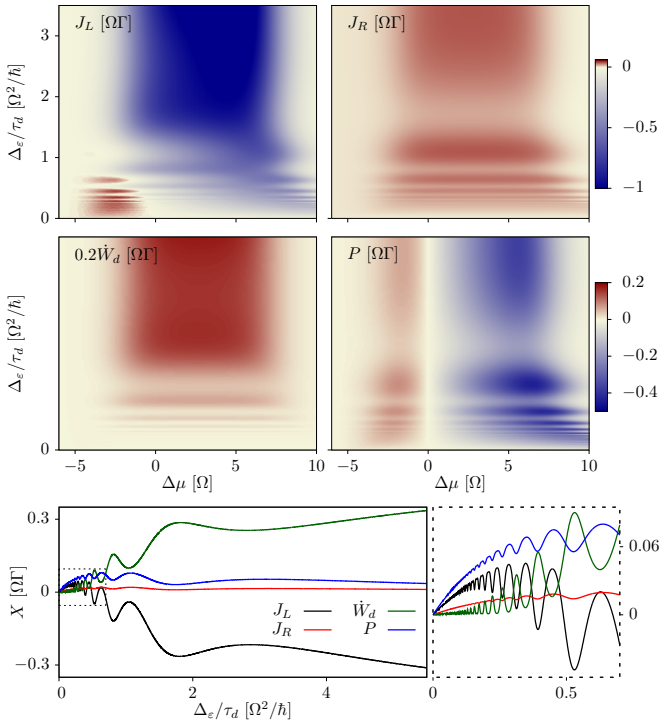


FIG. S3. Thermal currents $J_L$, $J_R$, $\dot{W}_d$ and $P$ as functions of the electrochemical potential bias and the driving speed, computed with the heuristic model for the same parameters used in Fig. S2. The lower panels plot cuts for fixed $\Delta\mu = -2.25\Omega$, the rightmost one zooming in the dotted square region.

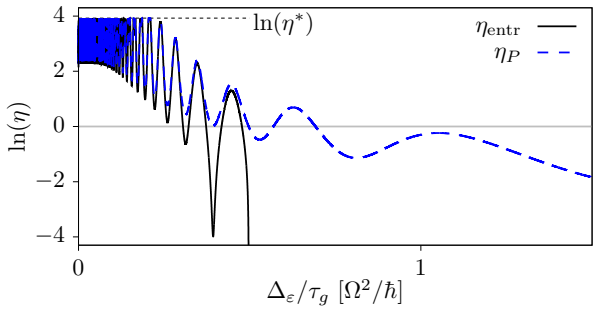


FIG. S4. Efficiency of the entropy reduction, $\eta_{\rm entrop}$, and power generation, $\eta_P$ processes as functions of the driving speed. The upper bound $\eta^*$ is given in the text.

current is suppressed (see Fig. S5): if $\mu_L > \varepsilon_0 + \Delta_\varepsilon$, the electron remaining in dot $l$ after a failed driving stage has an exponentially suppressed rate to tunnel out to L and therefore blocks the current (in this simplified model we are neglecting interdot tunneling after the drive).

### Efficiency

With Eqs. (S4)–(S6) we define different efficiencies, depending on whether the focus being put on violations of

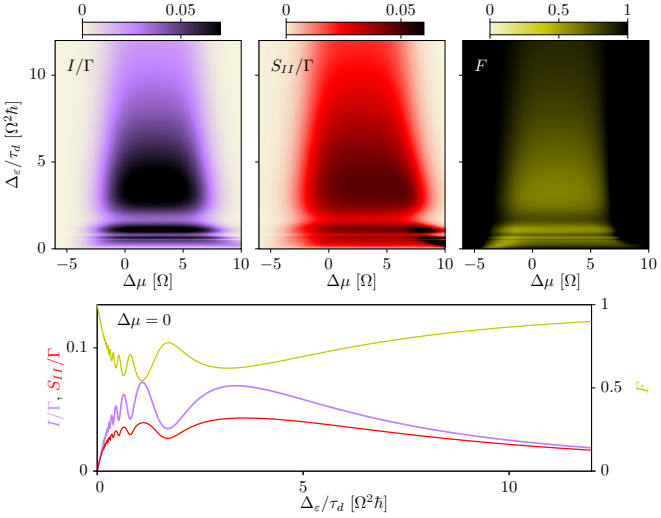


FIG. S5. Particle current, noise and Fano factor, $F = S_{II}/I$, computed with the heuristic model for the same parameters as in Fig. S2. The lower panel shows zero-bias cuts of the above quantities.

the second law:

$$\eta_{\rm entr} \equiv \frac{-\dot{S}_s T}{\dot{W}_d} \tag{S7}$$

or on power generation:

$$\eta_P \equiv \frac{P}{\dot{W}_d}. \tag{S8}$$

In the isothermal case ($T_L = T_R = T$), we get from energy conservation:

$$\eta_{\rm entr} = \eta_P - 1, \tag{S9}$$

with $\eta_P = (\mu_R - \mu_L)/\eta_{LZ}\Delta_\varepsilon$. In this sense, $\eta_{LZ}\Delta_\varepsilon$ defines the *probabilistic* resource expenditure of the demon. The demonic operations will correspond to having $\eta_{\rm entr} > 1$ or $\eta_P > 1$. In the adiabatic regime, $\eta_{LZ} \to 0$ makes the efficiencies huge and bounded by the system thermodynamic properties via the initial condition of the driving. Estimating that $P_{LZ}^{\rm ad} \approx f_L^0/(f_L^0 + f_R^\Delta)$, we find the upper bound $\eta_P \leq \eta^* = (\mu_R - \mu_L) f_L^0/\Delta_\varepsilon f_R^\Delta$, shown in Fig. S4. Errors in the driving reduce the efficiencies further. When they are below 1, the the demon operates correspondingly as a measurement-enabled heat engine or power transducer. For large driving speeds, entropy production becomes positive and the entropic demon stops working, while the power generation becomes increasingly inefficient.

### Noise

Using the heuristic master equation (S1), we can also calculate the zero frequency current noise, $S_{II}$ using full

counting statistics techniques [4]. The signal to noise ratio is given by the Fano factor, $F = S_{II}/I$. Superpoissonian regions (due to thermal fluctuations when transport is suppressed) are plotted in black. The result, plotted in Fig. S5, confirms that the zero-bias current is not only higher but also more regular in the intermediate regime. It becomes Poissonian in the adiabatic and highly nonadiabatic regimes, but for different reasons: in the adiabatic regime, the charge fluctuations are unidirectional and dominated by the coupling to the reservoirs, with transport being suppressed by the very long driving times; in the highly nonadiabatic regime, the driving becomes noisy and only few particles are successfully transferred to the right reservoir.


[1] G. T. Landi, M. J. Kewming, M. T. Mitchison, and P. P. Potts, Current Fluctuations in Open Quantum Systems: Bridging the Gap Between Quantum Continuous Measurements and Full Counting Statistics, PRX Quantum **5**, 020201 (2024).

[2] H. Sprekeler, G. Kießlich, A. Wacker, and E. Schöll, Coulomb effects in tunneling through a quantum dot stack, Phys. Rev. B **69**, 125328 (2004).

[3] P. P. Hofer, M. Perarnau-Llobet, L. D. M. Miranda, G. Haack, R. Silva, J. B. Brask, and N. Brunner, Markovian master equations for quantum thermal machines: local versus global approach, New J. Phys. **19**, 123037 (2017).

[4] R. Sánchez, G. Platero, and T. Brandes, Resonance Fluorescence in Transport through Quantum Dots: Noise Properties, Phys. Rev. Lett. **98**, 146805 (2007).